Optimization of a blueprint for in vitro glycolysis by metabolic real-time analysis

Bujara, Matthias; Schümperli, Michael; Pellaux, René; Heinemann, Matthias; Panke, Sven

Published in:
Nature Chemical Biology

DOI:
10.1038/nchembio.541

Supplementary information

Optimization of a blueprint for *in vitro* glycolysis by metabolic real-time analysis

Matthias Bujara[1], Michael Schümperli[2], René Pellaux[1,2], Matthias Heinemann[2,3], and Sven Panke[1, 2*]

[1]Department of Biosystems Science and Engineering, ETH Zurich, Mattenstrasse 26, 4058 Basel, Switzerland

[2]Institute of Process Engineering, Department of Mechanical and Process Engineering, ETH Zurich, Universitätsstrasse 6, 8092 Zurich, Switzerland

[3] Groningen Biomolecular Sciences and Biotechnology Institute, University of Groningen, Nijenborgh 4, 9747 AG Groningen, The Netherlands

[*]Corresponding author:

Sven Panke

Department of Biosystems Science and Engineering

ETH Zurich

Mattenstrasse 26

CH-4058 Basel

Switzerland

Email: sven.panke@bsse.ethz.ch
Tel.: +41-61-387 3209

Fax: +41-61-387 39 94

Nature Chemical Biology: doi:10.1038/nchembio.541

Content

Nature Chemical Biology: doi:10.1038/nchembio.541

1. Supplementary Results:

a) Flux control coefficient calculation from transient data

Supplementary Table 1: Coefficients 'α' from transient metabolite data using multiple linear regression according to equation (3) and calculation of flux control coefficients 'C' according to equation (2) (**Supplementary Methods**), More detailed information can be found in **Supplementary Methods**. The signal to noise ratio (S/N) of the FCCs was calculated to obtain an indication for the reliability. Except for HK and FBA, noise was higher than the actual signal.

No	R^2	Regression Coefficients								Flux Control Coefficients					
		const.	α_{GLUC}	$\alpha_{G6P/F6P}$	α_{FBP}	α_{DHAP}	$\alpha_{2/3PG/PEP}$	α_{PYR}	α_{ATP}	C_{HK}	C_{PFK}	C_{FBA}	C_{GAPDH}	C_{PK}	C_{LDH}
1	0.9993	4.5	-0.6	16.5	-5.8	95.7	0.5	17.0	-9.6	0.20	-0.09	0.75	-0.07	0.05	-0.13
2	0.9981	8.3	-0.4	8.8	-54.9	78.5	27.6	9.8	-16.4	0.17	-0.31	0.87	0.07	-0.22	-0.06
3	0.9985	5.3	-0.1	0.5	-35.9	65.2	36.2	33.5	-19.6	0.16	-0.13	0.79	0.13	-0.17	-0.26
4	0.9997	5.1	-0.4	16.1	4.7	121.0	-34.8	3.7	-11.0	0.18	0.00	0.78	-0.31	0.18	-0.02
5	0.9994	6.5	-0.5	11.6	-48.3	60.1	37.6	5.1	-18.7	0.20	-0.27	0.71	0.12	-0.34	-0.03
6	0.9981	-3.2	-0.6	59.0	19.5	83.8	14.7	14.4	13.4	0.33	-0.38	0.46	0.20	0.10	-0.10
7	0.9994	4.7	-0.4	17.8	2.4	112.9	-11.5	-2.2	-9.2	0.20	-0.05	0.81	-0.15	0.00	0.02
8	0.9997	4.6	-0.3	15.3	-1.3	109.1	-26.2	9.0	-11.1	0.18	-0.04	0.75	-0.25	0.16	-0.06
9	0.9993	5.4	-0.4	9.3	-6.0	98.4	-26.6	16.5	-13.5	0.17	-0.01	0.77	-0.30	0.22	-0.12
10	0.9997	4.3	-0.4	17.4	-6.7	93.9	-6.0	3.5	-8.7	0.18	-0.11	0.69	-0.10	0.01	-0.02
11	0.9994	6.7	-0.2	5.5	-11.3	106.8	-24.2	1.7	-15.1	0.16	-0.01	0.91	-0.30	0.08	-0.01
12	0.9977	5.4	-0.9	29.9	-52.4	52.4	63.2	16.4	-5.9	0.30	-0.62	0.85	0.46	-0.43	-0.13
									Mean (S)	0.18	-0.10	0.78	-0.08	0.03	-0.06
									Standard deviation (N)	0.05	0.19	0.11	0.24	0.21	0.08
									S/N	3.6	0.5	7.1	0.3	0.1	0.75

Nature Chemical Biology: doi:10.1038/nchembio.541

b) Enzyme sources and activities

Supplementary Table 2: Kinetic parameters of *E. coli*'s glycolytic enzymes and the commercially available glycolytic enzymes used for screening. The unit equivalent (U_{eq}) was calculated by determining the enzyme activity of commercially available enzymes under the reaction conditions used in this study. All units mentioned in this study refer to the activities reported here, not to the units given by the manufacturer. As glucokinase and hexokinase catalyze the same reaction, hexokinase (HK) was used as a synonym for glucokinase (Glk) to prevent confusion.

Enzyme	EC. No	Substrates	*E. coli enzymes*	Commercially available enzymes		
			$K_m^{(Ref.)}$ [mM]	$K_m^{(Ref.)}$ [mM]	Source	$U_{eq.}$[c]
Glucokinase/	2.7.1.2/	GLUC	0.5[1] – 3.76[2]	0.04[3] – 0.47[4]	*S. cerevisiae*	0.9
hexokinase	2.7.1.1	ATP	0.15[1] – 0.78[2]	0.1[5]		
Glucosephosphate isomerase	5.3.1.9	G6P	0.28[6]	0.3 – 1.5[7]	*S. cerevisiae*	n.d.
6-phosphofructo-	2.7.1.11	F6P	0.124[8, a]	0.023[9] – 0.03[10]	*B. stearothermophilus*	2.2
kinase		ATP	0.118[8, a]	0.07[10] – 0.12[9]		
Fructose-	4.1.2.13	FBP	0.175[8, a]	0.00084[11] – 0.01[12]	Rabbit muscle	1.0
bisphosphate aldolase						
Glyceraldehyde-3-	1.2.1.12	GAP	0.89[13]	0.09[14]	Rabbit muscle	n.d.
phoshate		NAD	0.45[13]	0.06[14]		
dehydrogenase		Pi	0.53[13]	n.a.		
Phosphoglycerate	2.7.2.3	1,3PG	n.a.	n.a.	*S. cerevisiae*	n.d.
kinase		ADP	n.a.	0.18[15]		
Pyruvate kinase	2.7.1.40	PEP	0.08 – 3.63[16, b]	n.a.	Rabbit muscle	n.d.
		ADP	0.3[16]			
D/L-lactate	1.1.1.27/	PYR	7.2[17]	0.76[18]	Rabbit muscle	0.9
dehydrogenase	1.1.1.28	NADH	7.0[17]	n.a.		

[a] geometric mean of available data as reported[8]
[b] depending on the concentration of the allosteric regulator FBP
[c] Unit equivalent: one manufacturer's unit corresponds to the indicated unit as measured under the conditions applied in this study
n.d. not determined, because the enzyme did not show any effect when added in excess
n.a. not available

Nature Chemical Biology: doi:10.1038/nchembio.541

c) Improved reproducibility after addition of HK and FBA

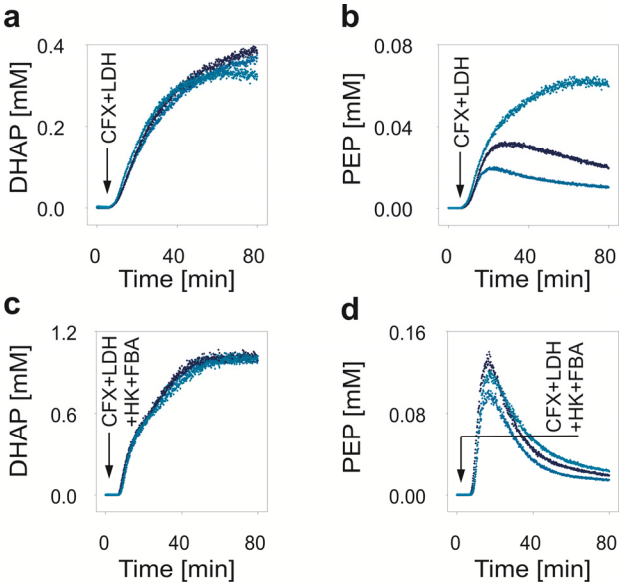

Supplementary Figure 1: Examples of DHAP and PEP time courses using aliquots of the same cell free extract without (**a-b**) and with addition of HK and FBA (**c-d**). Clearly, the system behavior becomes more reproducible after the addition of HK and FBA. DHAP and PEP curves were chosen as they represent extreme cases of good and bad reproducibility.

d) Coupling of the concentration time courses of 2PG/3PG and PEP

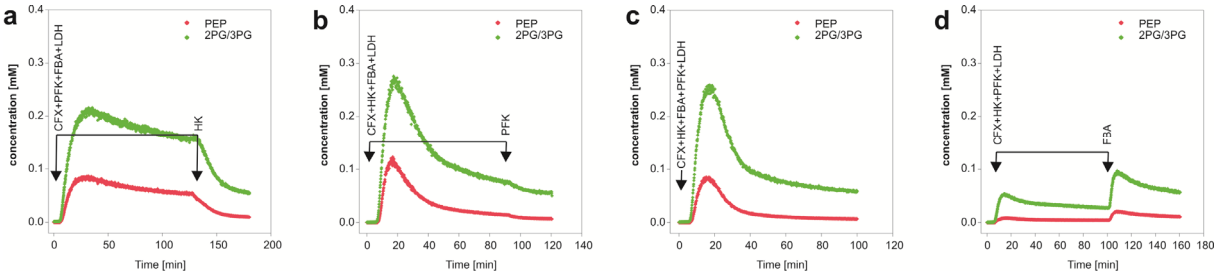

Supplementary Figure 2: The concentrations of metabolites 2PG/3PG and PEP are closely coupled. (**a-d**) Representative curves of 2PG/3PG and PEP time courses from experiments in which the supplementation of different combinations of purified HK, FBA and PFK showed that the 2PG/3PG and PEP concentrations are closely coupled.

Nature Chemical Biology: doi:10.1038/nchembio.541

e) Single enzyme perturbations in the lower part of glycolysis

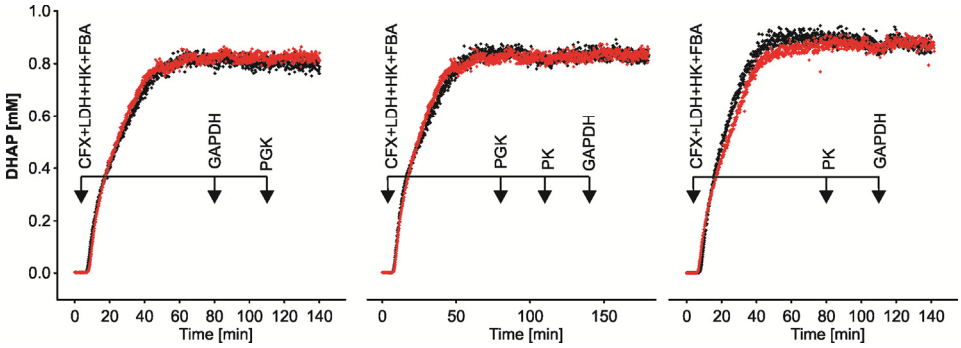

Supplementary Figure 3: Single enzyme perturbations in the lower part of glycolysis using *E. coli*'s *in vitro* optimized upper part of glycolysis (W3110 Δ*amn tpiA::kn*+LDH+HK+FBA) realizing all 8 possible combinations of additions of the enzymes GAPDH, PGK and PK suggested no rate limiting step in the lower part of glycolysis. Reactions were started by injection of CFX *in vitro* supplemented with enzymes from the upper part of glycolysis (5 U HK and 5 U FBA) followed by stepwise addition of enzymes of the lower part of glycolysis as indicated.

Nature Chemical Biology: doi:10.1038/nchembio.541

f) Modulation of FBA activity

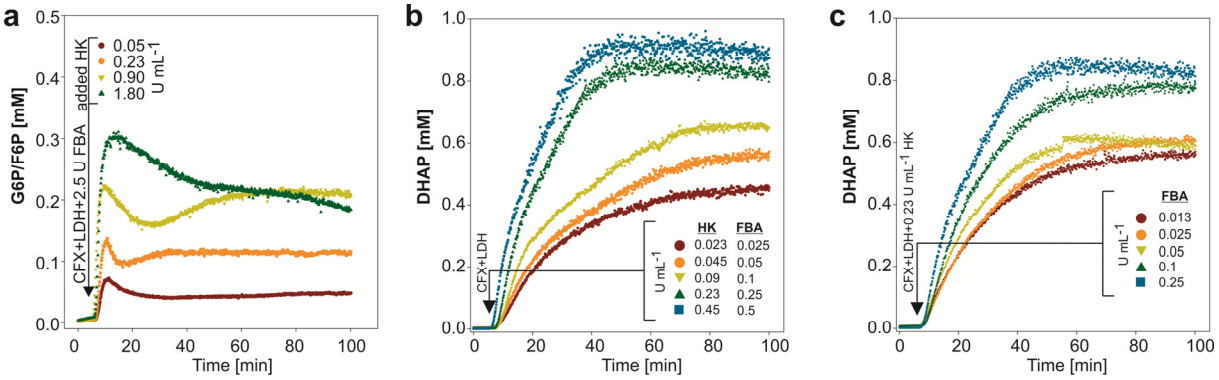

Supplementary Figure 4: Optimization of HK and FBA activities using commercially available enzymes and CFX from W3110 Δ*amn tpiA::Kn* by investigating the effect of enzyme additions on DHAP production. (**a**) An increase in HK activity leads to higher levels of G6P/F6P. (**b**) Simultaneous reduction of HK and FBA shows that a reduction by a factor of two is still sufficient for a 2.5-fold higher DHAP production compared to the non-optimized system. (**c**) Reduction of FBA activity while maintaining HK activity constant shows that further reduction to 0.1 U mL^{-1} is sufficient for DHAP production.

Nature Chemical Biology: doi:10.1038/nchembio.541

g) Analysis of the performance of operon *glk-fba-ldh* with pUC *ori*

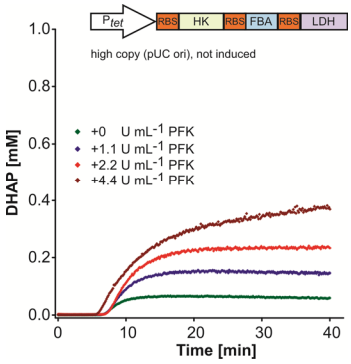

Supplementary Figure 5: Analysis for rate limiting steps using CFX from the operon-carrying *E. coli* W3110 Δ*amn tpiA::kn*. (**a**) Supplementation of CFX with commercially available PFK could elevate the production of DHAP. Enzyme activities refer to units (U) per mL reactor volume and were determined by an *in vitro* assay (**Supplementary Methods**).

h) Analysis of the performances of operon *glk-fba-ldh* with pBR322 ori and the operon *fba-ldh-glk* with pUC ori

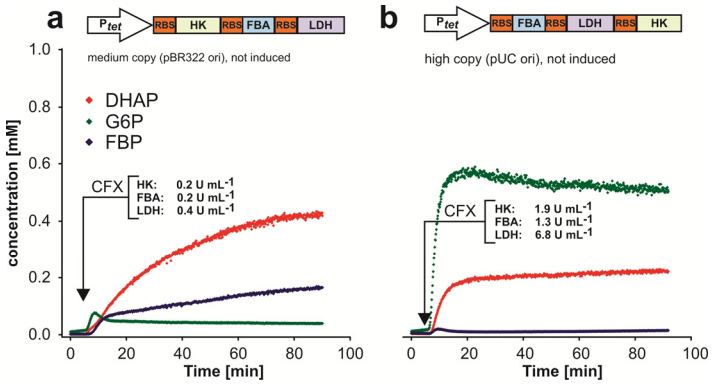

Supplementary Figure 6: Operon tuning for reducing HK activity. (**a**) Reduction of the copy number of the plasmid carrying the operon without induction shows similar DHAP production to CFX without operon expression. (**b**) Changing the order of genes in the operon did not lead to high DHAP production. In all cases CFX from *E. coli* W3110 Δ*amn tpiA::kn* was used. Enzyme activities refer to units (U) per mL reactor volume as determined by an *in vitro* assay (**Supplementary Methods**).

Nature Chemical Biology: doi:10.1038/nchembio.541

2. Supplementary methods:

a) Normalization by an internal standard: The absolute ion counts of the metabolites obtained from the enzyme-membrane reactor and measured in the MS are prone to fluctuations because of flow rate variations or day to day variations of the electrospray-ionization and therefore require normalization against an internal standard. We supplied 3-N-morpholino-propanesulfonic acid (MOPS) to the reactor feed medium, which is a biologically inert buffer and shows good signal intensity. Flow rate fluctuations can lead to a different dilution of the reactor outlet (fluctuations at S1) or to a different flow rate in the ESI ion source (fluctuations at S2). We have measured the flow rate of the waste streams of our reactor setup which allowed an estimated on the flow splitting at S1 and S2 (**Fig. 1**). We could not detect any major fluctuations at these mixing tees. However, the splitting ratio was not recorded online in the final measurement setup and could theoretically change over the course of an experiment. We therefore analyzed whether an internal standard can compensate for flow-rate fluctuations within in the setup. We doubled or halved the standard flow rates and recorded the influence on MOPS-normalized signals. As shown in **Supplementary Fig. 7**, the influence of the flow rate fluctuations in this setup was minor for fluctuations at S1 (**Supplementary Fig. 7a).** It should be emphasized that a different flow rate (by a factor of 2) at S1 doubles or halves the total concentration of e.g. G3P that is measured in the MS after dilution. Normalization against MOPS after a doubled or halved flow rate at S1 only shows a difference in normalized signal intensity of roughly 10% which is rather low compared to twice or half of the G3P signal without normalization. Given the large fluctuations imposed in this control experiment, we felt that these influences were acceptable. The influence of fluctuations at S2 was negligible (**Supplementary Fig. 7b)**. In summary, normalization against an internal standard compensates for flow-rate fluctuations

Nature Chemical Biology: doi:10.1038/nchembio.541

within the setup and consequently, varying total ion counts do not impair the measurements.

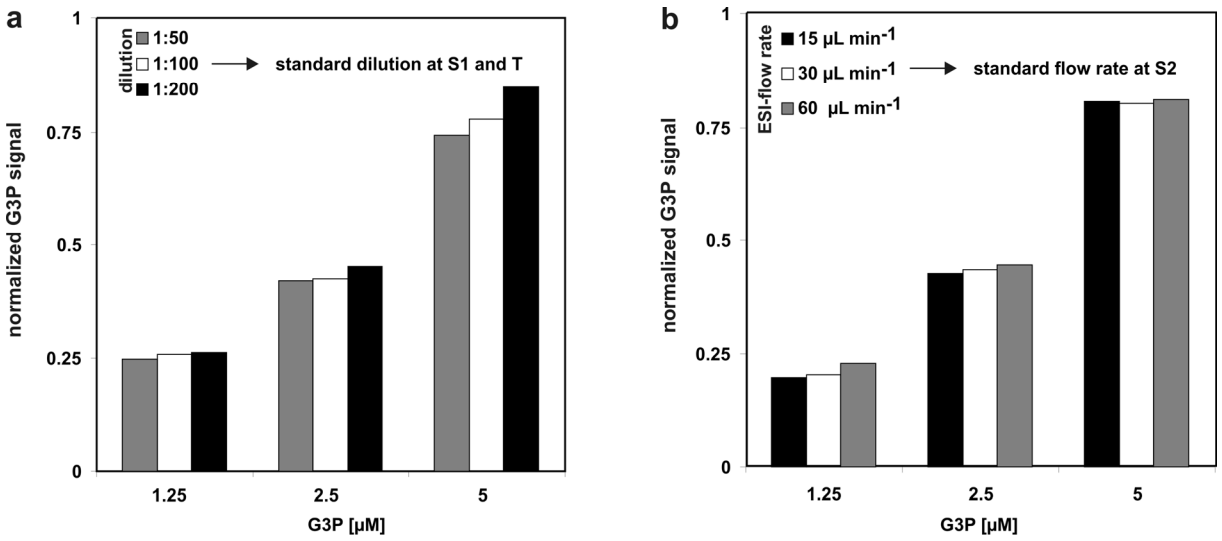

Supplementary Figure 7: Compensation of flow rate fluctuations within the setup by normalization against MOPS. (**a**) Flow rate fluctuations by a factor of two at S1 lead to a different dilution ratio of the reactor outlet, which can be compensated for by normalization against an internal standard. Note that the applied flow rate fluctuations are rather drastic. (**b**) Flow rate fluctuations by a factor of two at S2 leading to lower or higher flow rates into the ESI ion-source do not influence the normalized signal.

b) Calibration and quantification. Multi-enzyme network dynamics show changes in metabolite concentrations over several orders of magnitude. As the setup developed in this study operates at a fixed dilution rate, calibration curves over a broad concentration range were essential. Calibration for online quantification was performed using a syringe pump operated at 30 µL min^{-1} using three standard mixes containing five compounds at 1 mM. By splitting the calibration mix in three, we could prevent experimentally unrealistically high total ion concentrations. Standard mixes were prepared from pure compound stock solutions (50 mM stock solutions in water)

Nature Chemical Biology: doi:10.1038/nchembio.541

and frozen in aliquots at -80 °C. The standard mixes were diluted in calibration buffer which had a similar salt concentration as for online analysis (75% MeOH; 5 mM NH_4COOH; pH 4.8; 0.025 mM $MgCl_2$; 0.02 mM Na_2HPO_4; 0.5 mM NH_4HCO_3; 4 µM MOPS). Signal intensities of the different compounds were normalized against the MOPS signal and then used for quadratic regression. The limit of detection (LOD) and limit of quantification (LOQ) were calculated using a signal to noise ratio of 3 and 10, respectively.

To obtain concentration values from raw data the ion current from each compound is normalized against the ion current of MOPS. The normalized value is then converted to concentrations using a corresponding normalized calibration curve and the dilution factor is included to obtain real reactor concentrations.

To meet the demand for a broad quantification range, quadratic calibration curves were established (**Supplementary Table 3**) since the calibration curves for most compounds only showed a linear behavior up to a concentration of approximately 10 µM at the ion source (data not shown). As the coefficients of the quadratic terms were generally two orders of magnitude smaller than those of the linear terms, they only became relevant for high compound concentrations, meaning that they were essentially zero for very low concentrations. Using quadratic calibration curves allowed us to cover a concentration range of at least three orders of magnitude for all compounds with a maximum reactor concentration of 2.5 mM. An exception was glucose which covered a range up to 5 mM and NADH which covered a range up to 1.25 mM. Within these ranges quantification errors were generally smaller than 10% regardless whether high or low concentrations were considered.

Nature Chemical Biology: doi:10.1038/nchembio.541

Supplementary Table 3: Calibration data for glycolytic intermediate quantification. Limit of detection (LOD, at a signal to noise ration of S/N=3) and limit of quantification (LOQ, S/N=10) refer to concentrations in the reactor; hence, the concentrations measured at the ion-source are 100 times lower. Regression data were obtained by fitting to a quadratic calibration curve $y=ax^2+bx$. Note that the coefficient in the quadratic term is always two to three orders of magnitude smaller than the coefficient in the linear term, indicating that the quadratic term is only a small correction for high metabolite concentrations. A 3PG calibration curve was used to quantify the overlapping 2PG/3PG pool and G6P to quantify the overlapping G6P/F6P pool (see also 1d).

	LOD [mM]	LOQ [mM]	R^2	a [mM^{-2}]	b [mM^{-1}]
PYR	3.65E-02	6.05E-02	0.9998	2.61E-05	3.92E-03
LAC	6.89E-01	1.69E+00	0.9997	2.86E-05	4.31E-03
PEP	4.84E-04	9.44E-04	>0.9999	-3.50E-04	1.63E-01
DHAP	2.34E-03	7.33E-03	0.9999	-8.43E-04	1.69E-01
GAP	1.44E-03	3.19E-03	>0.9999	-4.09E-05	6.94E-03
G3P	2.08E-03	4.03E-03	0.9999	-7.50E-04	1.65E-01
GLUC	3.20E-02	1.02E-01	>0.9999	-1.16E-04	1.60E-02
2PG	4.29E-03	1.31E-02	0.9999	-5.52E-04	1.33E-01
G6P	1.39E-03	3.30E-03	0.9998	-1.59E-03	1.80E-01
FBP	8.21E-04	1.67E-03	0.9998	-1.05E-03	1.65E-01
AMP	1.40E-03	3.23E-03	>0.9999	-7.86E-05	3.44E-02
ADP	1.02E-02	2.37E-02	>0.9999	-3.95E-04	8.06E-02
ATP	2.79E-03	6.41E-03	0.9998	2.75E-04	2.27E-02
NAD	2.47E-03	6.30E-03	>0.9999	-1.78E-03	1.28E-01
NADH	2.98E-03	9.86E-03	0.9998	-2.90E-04	2.93E-02

c) Compensation of MS-signal overlaps. Since direct injection ESI-MS analysis without chromatographic separation was performed, overlapping MS-signals needed to be resolved. Overlapping signals have been reported previously[19,20] and can occur if MRM transitions are not specific for a certain compound. For the set of metabolites analyzed here, the two compound sets G6P/F6P as well as 2PG/3PG could not be

Nature Chemical Biology: doi:10.1038/nchembio.541

distinguished from each other since they showed exactly the same fragmentation patterns and intensities. Subsequently, only the G6P/F6P and 2PG/3PG pools rather than individual concentrations were determined in the following analyses.

The two compounds FBP and GAP showed overlapping signals at the MRM transition of DHAP (**Supplementary Fig. 8a**) but could be distinguished from DHAP using unique fragment ions. The “false positive” signal of FBP at the DHAP transition was very low and could be neglected. The “false positive” signal of the phosphate ion of GAP at the DHAP transition was only 30% lower than the DHAP signal itself (**Supplementary Fig. 8a**). Here, a unique fragmentation pattern of GAP could be used for its exact quantification and allowed for calculating the contribution of the overlapping GAP signal. To confirm this, we measured first samples containing equimolar amounts of GAP and DHAP, which showed, as expected, higher signals at the DHAP-transition compared to samples containing the same amount of DHAP only. When the overlapping GAP signal was subtracted from the signal of the equimolar mixture, the corrected values were identical to those measured for DHAP alone, indicating that the correction method was accurate (**Supplementary Fig. 8b**). In this study, the DHAP signal was corrected for the overlapping GAP signal as soon as GAP could be quantified in the sample. However, please note that in the vast majority of scenarios described here, the GAP concentration remained below the LOQ and correction was therefore not necessary. However, we can correct the signal for false positive fractions in case reliable GAP concentrations are measured in future experiments.

A similar observation was made for the NAD^+ and NADH signals. NADH showed an overlapping signal with the MRM-transition of NAD^+, which could be corrected by subtracting the false positive signal of NADH, as shown by the identity of a curve obtained from NAD^+ alone and one obtained from measuring the NAD^+ signal from

Nature Chemical Biology: doi:10.1038/nchembio.541

an equimolar mix of NAD^+ and NADH and then subtracting the NADH-specific contribution (**Supplementary Fig. 8c-d**). In this study, the NAD^+ signal was corrected for the overlapping NADH signal when NADH was present above the LOQ.

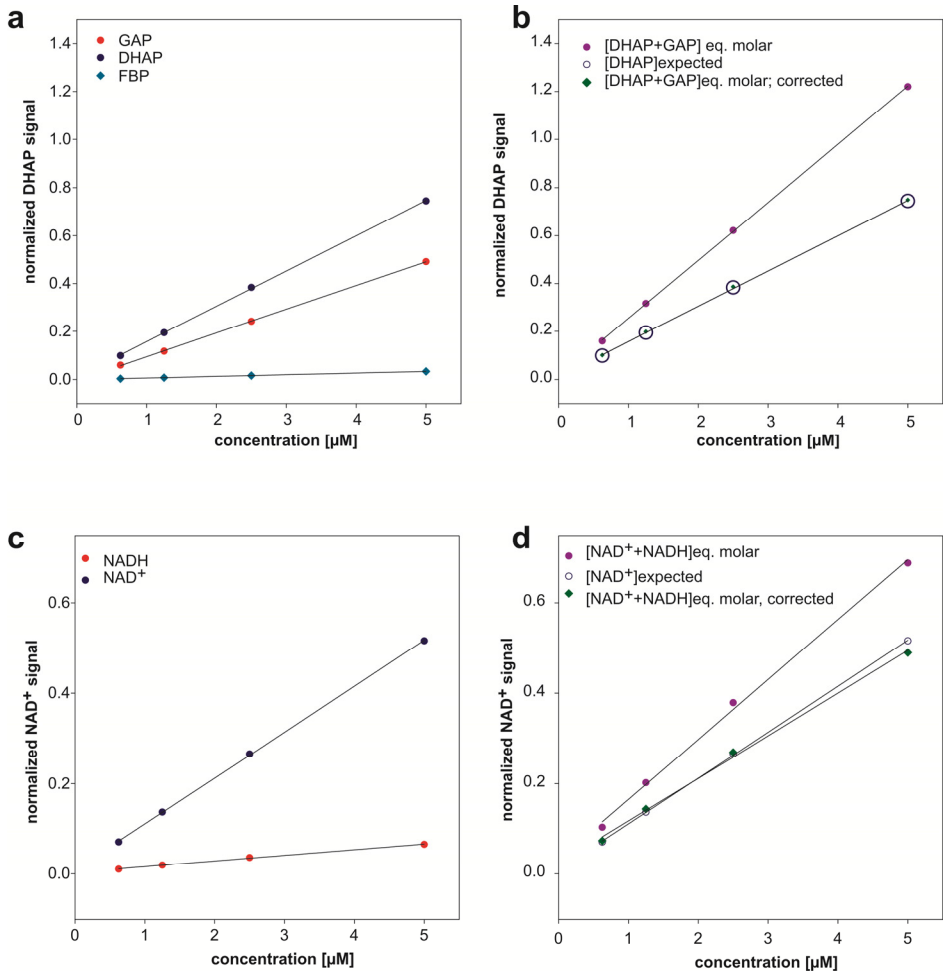

Supplementary Figure 8: Correction of overlapping signals of the compound sets DHAP-GAP and NAD^+-NADH. (**a**) Normalized DHAP signal at the MRM-transition of DHAP and the "false positive signal" ratios of FBP and GAP at the same transition. (**b**) The "false positive" contribution of the GAP signal at the DHAP transition can be accurately corrected by subtraction, as shown by subtracting the GAP signal (evaluated at a different and unique MRM transition) from the joint DHAP/GAP signal at the DHAP transition. (**c**) "False positive" signal of NADH at the MRM-transition of NAD^+. (**d**) Correction of the "false positive" NADH signal at the NAD^+-transition:

Nature Chemical Biology: doi:10.1038/nchembio.541

Subtraction of the false positive NADH signal (evaluated at a different and unique MRM transition) from the signal obtained for equimolar amounts of NAD^+ and NADH coincides with the curve obtained for NAD^+ only.

d) Analysis of ion-specific matrix effects. The effect of ion suppression is a well known phenomenon in ESI-MS analysis and can be regarded as the major limitation for the method[21]. An understanding of the impact of ion suppression is essential for the validation of the presented method[21] and particularly for online measurement of glycolytic intermediates since the quantitative measurements will be performed in a dynamically changing matrix without prior chromatographic separation. In order to analyze potential matrix effects, standard addition of pure compounds to two physiological samples from *in vitro* batch conversion of glucose and ATP was performed as reported previously[22]. Briefly, two samples were taken (after 30 min and 120 min) from a 10 mL batch reaction at 37°C (100 mM $NaHCO_3$ pH 7.7; 5 mM $MgCl_2$; 0.8 mM KCl; 11.1 mM GLUC; 11.1 mM sodium phosphate pH 7.7; 5.75 mM NAD^+; 1 mg mL^{-1} CFX (W3110 Δ*amn tpiA::kn*); 11.1 mM ATP). The reaction was inactivated by adding one volume of isopropanol and chilling on ice, precipitated proteins were removed by centrifugation. The supernatant was diluted 1:500 in calibration buffer (75% MeOH; 5 mM NH_4COOH; pH 4.8; 0.025 mM $MgCl_2$; 0.02 mM Na_2HPO_4; 0.5 mM NH_4HCO_3; 4 µM MOPS) which contained various compounds at different concentrations that were typical for our experiments. To these samples the specific compound was added from a 100-fold stock solution in different concentrations yielding final added concentrations of 0.625; 1.25; 2.5 and 5 µM. Samples were analyzed using a syringe pump at 30 µL min^{-1}. The increase in signal for the specific compound was determined, leading to two calibration curves (one for each original sample) with different intercepts on the ordinate depending on how

much of the specific compound was in the original sample to start with. Such standard addition curves were recorded for all compounds in both samples (**Supplementary Fig. 9**). As normalized signal intensities were still in the linear range, experiments were evaluated by calculating the relative deviation of the slope (in percent) of standard addition experiments in the two matrices.

The effect of ion suppression for the specific compound was then estimated from the ratio of the two calibration curves, each recorded in a different but still typical concentration matrix (**Supplementary Table 4**). In the absence of any ion suppression effect, the two slopes should be identical irrespective of the background; the ratio of the two slopes should be 1 (100%). The obtained slope ratios varied between 94.7% for pyruvate and 106.5% for ADP. In summary, these results indicated that in the system under study ion suppression effects were only a minor issue, as slopes were nearly identical and the added compounds only showed a minor impact onto the signals of the non-added compounds (**Supplementary Fig. 9**).

Nature Chemical Biology: doi:10.1038/nchembio.541

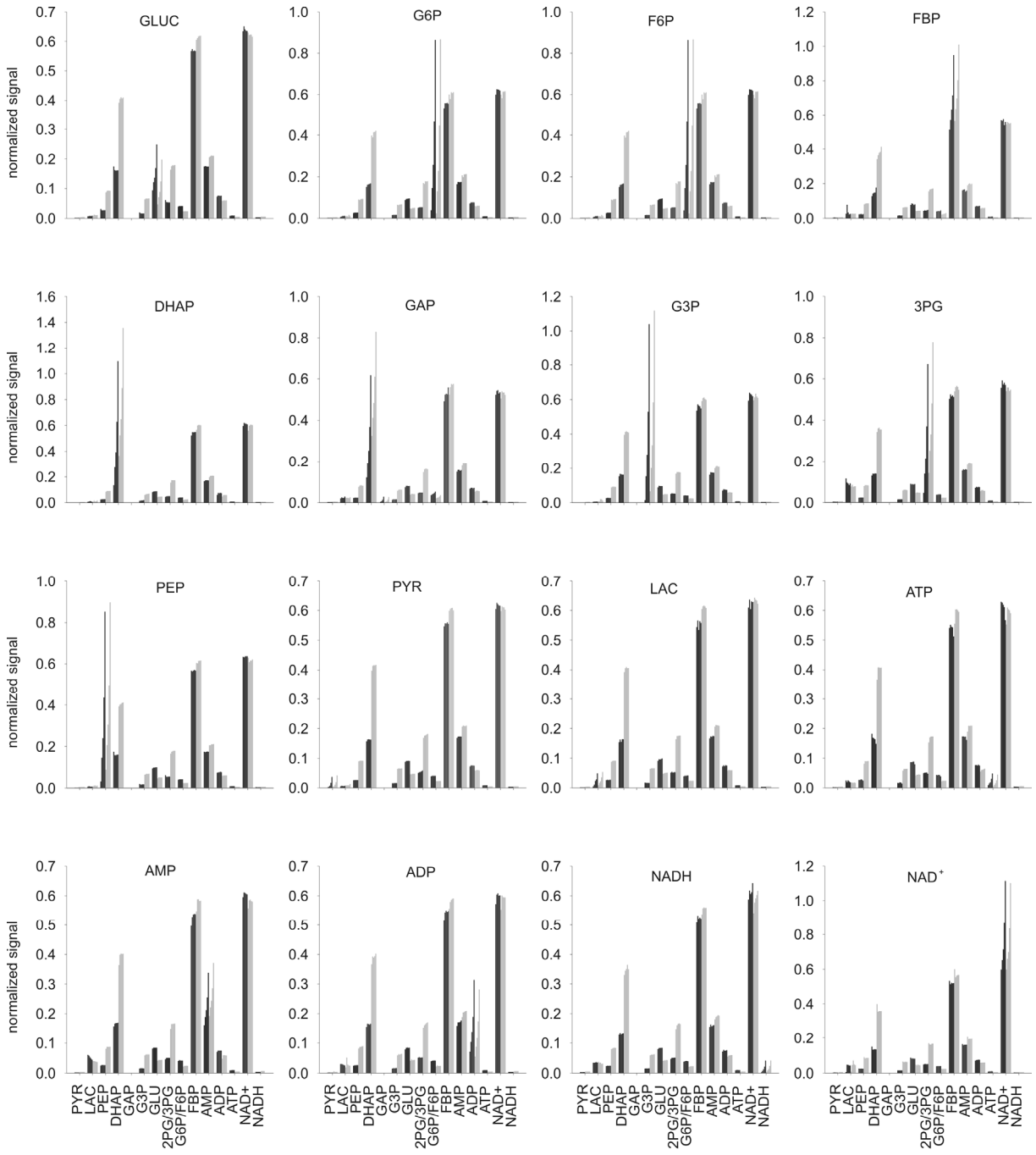

Supplementary Figure 9: Analysis of ion-suppression by standard addition experiments for 16 different compounds. The respective compound was added to 0.625, 1.25, 2.5 and 5 µM to two different samples (black and grey) obtained at two different time points from DHAP production experiments with an *E. coli in vitro* glycolysis. Note that these added concentrations reflect the situations in the ionization chambers, concentrations in the reactor are consequently 100 times higher. Normalized signal intensities of the respective compound and the recorded

Nature Chemical Biology: doi:10.1038/nchembio.541

signal intensities of the non-added compounds are shown (in total 10 signal intensities per compound: two experiments, five measurements each (first, no addition, and then 4 additions of the specific compound). Note that the two sets of concentration for the added compound have to differ, as the two samples used for standard addition contained different concentrations of the corresponding compound. The two slopes for the added compound were calculated and the slope ratio is shown in **Supplementary Table 4**.

Supplementary Table 4: Analysis of ion suppression for the glycolytic intermediates studied. Standard additions (0.625; 1.25; 2.5; 5 µM, concentrations as injected in the ESI-chamber) of each compound were performed to two different samples and the ratio of the two slopes of signal over concentration is shown.

compound	**PYR**	**LAC**	**PEP**	**DHAP**	**GAP**	**G3P**	**GLUC**	**2PG**
slope ratio [%]	94.7	95.7	101.9	97.8	103.5	97.5	101.2	99.4

compound	**G6P**	**F6P**	**FBP**	**AMP**	**ADP**	**ATP**	**NAD^+**	**NADH**
slope ratio [%]	97.7	97.7	97.6	99.4	106.5	98.9	103.8	102.0

e) Characterization of the metabolic real-time analysis setup. For an accurate quantification during rapid concentration changes, it is important to know whether the concentrations measured in the MS truly reflect the concentrations in the reactor or whether the passage of the fluid through splitting and mixing tees has significantly influenced the shape of the curves of concentration over time. The impact of the different parts of the setup (reactor, dilution device and membrane) was characterized by analyzing the concentration over time of a tracer pulse at the MS. For all experiments G3P was used as a tracer and MOPS was used as the internal standard. The signal was quantified after normalization using a standard curve for

Nature Chemical Biology: doi:10.1038/nchembio.541

G3P recorded at the corresponding flow rate at the ESI ion source (30 µL min^{-1} for experiments with the dilution device and 250 µL min^{-1} for experiments without the dilution device). The feed solution was 400 µM MOPS in pure water for experiments with the dilution device which was then diluted with matrix buffer (75% MeOH, 5 mM NH_4COOH, pH 4.8). Without the dilution device matrix buffer with 4 µM MOPS was used.

The reactor itself showed a dead time of 0.5 min when operated without the dilution device (S1, T, and S2, see **Fig. 1**). The dilution device prolonged the dead time by 1 min because of the tubing. The concentration time course obtained due to the residence time distribution in the reactor was hardly changed by the dilution device, indicating that the dilution did not cause significant disturbances of the signal. When the reactor was fitted with a membrane to retain the enzymes of the CFX, the curve flattened slightly and showed a retarded peak, but residence time profiles were reproducible for the 10 glycolytic metabolites and 5 cofactors studied here (**Supplementary Fig. 10**). We are currently working on protocols for the mathematical correction of this slight change in signal from reactor interior to ESI-chamber, but argue that this minor effect is of no relevance for the results presented in this work.

Once the separate items of the setup had been characterized with G3P only, the results were confirmed for all compounds with the final setup. Here, the dynamics of 200 µL pulses of 4 compounds (12.5 µM each) was recorded for 1 h. Primary data were first normalized against MOPS and are shown as signal intensities relative to the maximum signal intensity of each compound (**Supplementary Fig. 10b**).

Nature Chemical Biology: doi:10.1038/nchembio.541

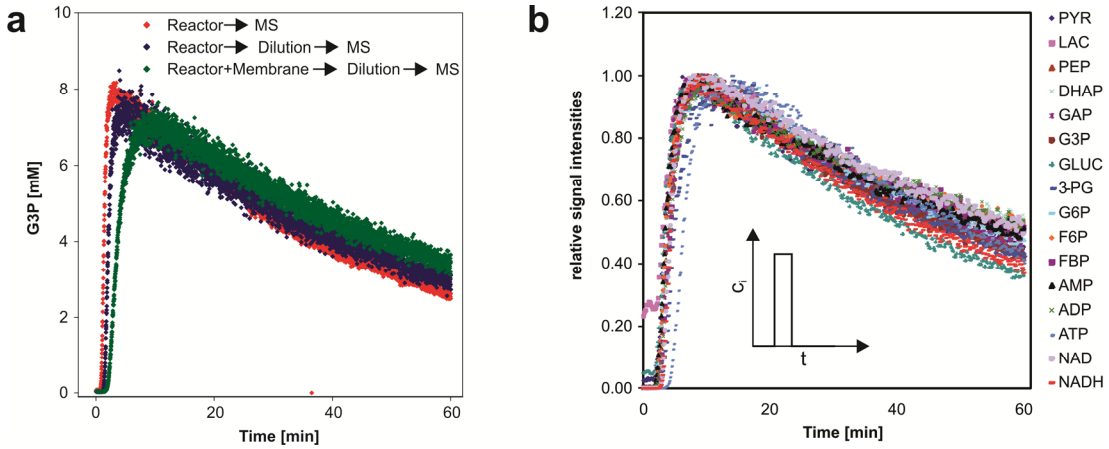

Supplementary Figure 10: Dynamic behavior of the reactor setup. (**a**) Residence time profile of a G3P pulse of the setup operated with and without the dilution device and with a membrane. (**b**) Relative residence time profiles of investigated metabolites, normalized to their maximum intensity.

f) Measuring frequency. In this study 15 compounds plus MOPS as an internal standard were analyzed in parallel, which means that the measurement time (dwell time) for each compound has an impact on time-resolution. Therefore, the impact of measuring frequency on data quality after normalization against the internal standard was analyzed. The signal to noise ratio at dwell times per compound of 5 to 2500 ms, which corresponds to time-resolutions between 6.3 Hz and 0.02 Hz (based on the analysis of 16 compounds), was analyzed and revealed better data quality for lower time-resolutions (**Supplementary Fig. 11**). The beneficial effect of longer dwell times becomes obvious at a dwell time of 1000 ms and 2500 ms, where the noise is about 60 to 100 times lower than the signal. The analysis in this study was performed at 0.125 Hz (7.5 measurements per minute) which in our view was a good tradeoff between data density and signal quality, but an increase in time-resolution by a factor of five would be easily possible if required, with only minor consequences for data

Nature Chemical Biology: doi:10.1038/nchembio.541

quality. Higher time-resolutions would be also possible, but only at the expense of data quality.

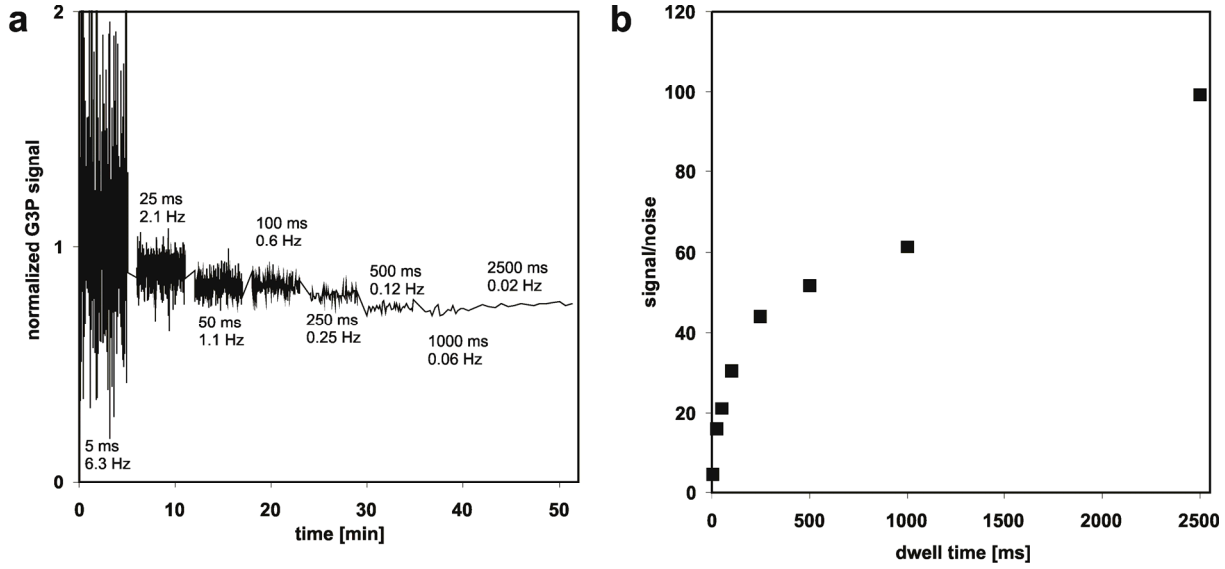

Supplementary Figure 11: The impact of measurement frequency on data quality. (**a**) Signal stability of the normalized G3P/MOPS signal at different dwell times or time-resolutions (in Hz, based on 16 MRM transitions). (**b**) Signal to noise ratio at different dwell times. The standard deviation of the normalized ion count was used as a measure for the noise and the mean as signal.

g) Calculation of flux control coefficients. Flux control coefficients (FCCs) from dynamic metabolite time courses were calculated as described previously[23,24]. The method has two limitations: First, it assumes linear rate equations in the relevant substrate concentration ranges, which is not necessarily the case. However, the influence of non-linearity is usually limited[24]. Second, the method is sensitive to measurement inaccuracies[25]. However, we argue that this problem is eliminated to a large extent by metabolic real-time analysis, which gives continuous, high frequency data with high consistency when compared to traditional enzyme-based assays or

Nature Chemical Biology: doi:10.1038/nchembio.541

discretely withdrawn samples for HPLC-MS analysis. Briefly, the method is applied as follows: a set of coefficients α_j can be calculated for a K-enzyme pathway from transient metabolite time courses by multiple linear regression of time (t) on the dynamic time course $c_j(t)$ according to Eq. (1).

$$\sum_{j=1}^{K} \alpha_j \left(c_j(t) - c_j(0) \right) = t \qquad (1)$$

The FCCs of the pathway are related to α_j via the steady state flux J and stoichiometric matrix S.

$$\left(C_1^J \; C_2^J \; \ldots \; C_L^J \right) = (\alpha_1 \; \alpha_2 \; \ldots \; \alpha_K) * S * J \qquad (2)$$

For FCC calculation the time period from 5.5 – 19 min from **Fig. 3** comprising 100 data points was used which showed the largest dynamic changes, thereby minimizing the collinearity of regression coefficients.

For the pathway studied here, the following assumptions were made: G6P and F6P are in equilibrium and were lumped into one reaction; 2PG/3PG and PEP were in equilibrium (**Supplementary Fig. 2**) and are also lumped into one reaction; as GAP was always below the LOQ it was assumed to react rapidly to 1,3-PG and therefore GAP-DH and PGK were also lumped into one reaction. The reactions from ADP to AMP as well as from DHAP to G3P were neglected and consequently the pathway was treated as linear. As the NAD^+ time course was constant it could be considered as a constant external metabolite and was therefore omitted from FCC calculation. Based on these assumptions the pathway can be described by the following stoichiometric matrix:

Nature Chemical Biology: doi:10.1038/nchembio.541

	HK	PFK	FBA	GAPDH	PK	LDH
GLUC	-1	0	0	0	0	0
G6P	1	-1	0	0	0	0
FBP	0	1	-1	0	0	0
DHAP	0	0	1	0	0	0
GAP/1,3PG	0	0	1	-1	0	0
2/3PG/PEP	0	0	0	1	-1	0
PYR	0	0	0	0	1	-1
LAC	0	0	0	0	0	1
ATP	-1	-1	0	1	1	0
ADP	1	1	0	-1	-1	0

For the calculation of the regression coefficients α_j, the regression coefficient $\alpha_{GAP/1,3PG}$ was set to zero as it could not be measured, α_{LAC} was set to zero as LAC was below the LOQ and α_{ADP} was set to zero to avoid collinearity of ATP and ADP because of the mass balance equation. Considering starting concentrations of ATP and GLUC by a constant term, Eq. (1) can be written as:

$$\alpha_{GLUC}c_{GLUC}(t) + \alpha_{G6P/F6P}c_{G6P/F6P}(t) + \alpha_{FBP}c_{FBP}(t) + \alpha_{DHAP}c_{DHAP}(t) + \alpha_{2/3PG/PEP}c_{2/3PG/PEP}(t) + \alpha_{PYR}c_{PYR}(t) + \alpha_{ATP}c_{ATP}(t) + const = t \quad (3)$$

The steady state DHAP flux was calculated by dividing steady state DHAP concentrations through the residence time τ=40 min. FCCs could then be calculated by applying Eq. (1).

h) Full factorial set of perturbations. All possible combinations of enzyme additions were realized in order to analyze the influence of each combination on DHAP production. This could be performed in six metabolic real-time analysis runs (**Supplementary Table 5**) by adding the next enzyme when steady concentrations of DHAP were reached.

Nature Chemical Biology: doi:10.1038/nchembio.541

Supplementary Table 5: Full factorial experimental design for all 16 possible combinations of single enzyme additions. The 16 combinations can be realized in 6 experiments (a-f) by stepwise addition of enzymes in each experiment (in the order according to subscripts).

	No.	HK	PGI	PFK	FBA
	1	-	-	-	-
a	**2**	$+_1$	-	-	-
	3	+	$+_2$	-	-
	4	+	+	$+_3$	-
b	**5**	-	-	$+_1$	-
	6	-	-	+	$+_2$
	7	$+_3$	-	+	+
c	**8**	-	$+_1$	-	-
	9	-	+	$+_2$	-
	10	-	+	+	$+_3$
d	**11**	-	-	-	$+_1$
	12	-	$+_2$	-	+
	13	$+_3$	+	-	+
	14	+	+	$+_4$	+
e	**15**	$+_1$	-	$+_2$	-
f	**16**	$+_1$	-	-	$+_2$

i) Activity measurements. Enzyme activities were determined spectrophotometrically in a temperature controlled (30°C) 96-well plate reader (Perkin Elmer, Waltham, Massachusetts, USA) by measuring the production/consumption of NAD^+/NADH or $NADP^+$/NADPH via a change in the absorbance at 340 nm. All assays were performed in 50 mM NH_4HCO_3; 2.5 mM $MgCl_2$. Enzyme-specific conditions were as follows: HK: 5 mM glucose, 2.5 mM ATP, 0.5 mM $NADP^+$, 1.75 U mL^{-1} glucose-6-phosphate dehydrogenase; PFK: 5 mM fructose-6-phosphate, 2.5 mM ATP, 0.5 mM NADH 1.7 U mL^{-1} glycerol-3-phosphate dehydrogenase, 0.4 U mL^{-1} fructosebisphosphate aldolase; FBA: 5 mM

Nature Chemical Biology: doi:10.1038/nchembio.541

fructosebisphosphate, 0.5 mM NADH, 1.7 U mL^{-1}; LDH: 5 mM pyruvate, 0.5 mM NADH. The slope of the linear part of the curve recorded at 340 nm and the protein concentration was used to calculate the specific enzyme activity in the CFX. The activities of commercially available enzymes were different from those given by the supplier and the conversion factors can be found in **Supplementary Table 2**.

3. Supplementary References:

1. Arora, K.K. & Pedersen, P.L. Glucokinase of *Escherichia coli*: Induction in response to the stress of overexpressing foreign proteins. *Arch. Biochem. Biophys.* **319**, 574-578 (1995).
2. Meyer, D., Schneider-Fresenius, C., Horlacher, R., Peist, R. & Boos, W. Molecular characterization of glucokinase from *Escherichia coli* K-12. *J. Bacteriol.* **179**, 1298-1306 (1997).
3. Fernandez, R., Herrero, P. & Moreno, F. Inhibition and inactivation of glucose-phosphorylating enzymes from *Saccharomyces cerevisiae* by D-xylose. *J. Gen. Microbiol.* **131**, 2705-2709 (1985).
4. Miller, S., Ross-Inta, C. & Giulivi, C. Kinetic and proteomic analyses of S -nitrosoglutathione-treated hexokinase A: consequences for cancer energy metabolism. *Amino Acids* **32**, 593-602 (2007).
5. Gao, H. & Leary, J.A. Multiplex inhibitor screening and kinetic constant determinations for yeast hexokinase using mass spectrometry based assays. *J. Am. Soc. Mass. Spectrom.* **14**, 173-181 (2003).
6. Schreyer, R. & Böck, A. Phosphoglucose isomerase from *Escherischia coli* K10: Purification, properties and formation under aerobic and anaerobic condition. *Arch. Microbiol.* **127**, 289-296 (1980).

Nature Chemical Biology: doi:10.1038/nchembio.541

7. Chang, A., Scheer, M., Grote, A., Schomburg, I. & Schomburg, D. BRENDA, AMENDA and FRENDA the enzyme information system: new content and tools in 2009. *Nucl. Acids Res.* **37**, D588-592 (2009).

8. Bennett, B.D. et al. Absolute metabolite concentrations and implied enzyme active site occupancy in *Escherichia coli*. *Nat. Chem. Biol.* **5**, 593-599 (2009).

9. Zhu, X., Byrnes, M., Nelson, J.W. & Chang, S.H. Role of glycine 212 in the allosteric behavior of phosphofructokinase from *Bacillus stearothermophilus*. *Biochemistry (Mosc).* **34**, 2560-2565 (1995).

10. Byrnes, M., Zhu, X., Younathan, E.S. & Chang, S.H. Kinetic characteristics of phosphofructokinase from *Bacillus stearothermophilus*: MgATP nonallosterically inhibits the enzyme. *Biochemistry (Mosc).* **33**, 3424-3431 (1994).

11. Pezza, J.A. et al. Spatial Clustering of Isozyme-specific Residues Reveals Unlikely Determinants of Isozyme Specificity in Fructose-1,6-bisphosphate Aldolase. *J. Biol. Chem.* **278**, 17307-17313 (2003).

12. Gavalda, S., Braga, R., Dax, C., Vigroux, A. & Blonski, C. N-Sulfonyl hydroxamate derivatives as inhibitors of class II fructose-1,6-diphosphate aldolase. *Biorg. Med. Chem. Lett.* **15**, 5375-5377 (2005).

13. Eyschen, J., Vitoux, B., Marraud, M., Cung, M.T. & Branlant, G. Engineered glycolytic glyceraldehyde-3-Phosphate dehydrogenase binds the anti conformation of NAD+ nicotinamide but does not experience A-specific hydride transfer. *Arch. Biochem. Biophys.* **364**, 219-227 (1999).

14. Lambeir, A.-M. et al. The cytosolic and glycosomal glyceraldehyde-3-phosphate dehydrogenase from *Trypanosoma brucei*. *Eur. J. Biochem.* **198**, 429-435 (1991).

Nature Chemical Biology: doi:10.1038/nchembio.541

15. Hurth, C. et al. Enzymatic activity of immobilized yeast phosphoglycerate kinase. *Biosens. Bioelectron.* **22**, 2449-2455 (2007).

16. Valentini, G. et al. The allosteric regulation of pyruvate kinase. *J. Biol. Chem.* **275**, 18145-52 (2000).

17. Tarmy, E.M. & Kaplan, N.O. Kinetics of *Escherichia coli* B D-lactate dehydrogenase and evidence for pyruvate-controlled change in conformation. *J. Biol. Chem.* **243**, 2587-2596 (1968).

18. Russell, P.J., Williams, A., Amador†, X. & Vargas†, R. Aldolase and Actin Protect Rabbit Muscle Lactate Dehydrogenase from Ascorbate Inhibition. *J. Enzyme Inhib. Med. Chem.* **19**, 91-98 (2004).

19. Soga, T. et al. Simultaneous determination of anionic intermediates for *Bacillus subtilis* metabolic pathways by capillary electrophoresis electrospray ionization mass spectrometry. *Anal. Chem.* **74**, 2233-2239 (2002).

20. Luo, B., Groenke, K., Takors, R., Wandrey, C. & Oldiges, M. Simultaneous determination of multiple intracellular metabolites in glycolysis, pentose phosphate pathway and tricarboxylic acid cycle by liquid chromatography-mass spectrometry. *J. Chromatogr. A* **1147**, 153-164 (2007).

21. Taylor, P.J. Matrix effects: The Achilles heel of quantitative high-performance liquid chromatography-electrospray-tandem mass spectrometry. *Clin. Biochem.* **38**, 328-334 (2005).

22. Bujara, M., Schümperli, M., Billerbeck, S., Heinemann, M. & Panke, S. Exploiting cell-free systems: Implementation and debugging of a system of biotransformations. *Biotechnol. Bioeng.* **106**, 376-389 (2010).

23. Delgado, J. & Liao, J.C. Determination of Flux Control Coefficients from transient metabolite concentrations. *Biochem. J* **282**, 919-927 (1992).

24. Delgado, J. & Liao, J.C. Metabolic control analysis using transient metabolite concentrations. Determination of metabolite concentration control coefficients. *Biochem. J* **285**, 965-972 (1992).

25. Ehlde, M. & Zacchi, G. Influence of experimental errors on the determination of flux control coefficients from transient metabolite concentrations. *Biochem. J* **313**, 721-727 (1996).

Nature Chemical Biology: doi:10.1038/nchembio.541